

# Spin texture tunability in $\text{Mn}_{1-x}\text{Ge}_x\text{Bi}_2\text{Te}_4$ through varying Ge Concentration

A.M. Shikin,<sup>1,\*</sup> D.A. Estyunin,<sup>1</sup> N.L. Zaitsev,<sup>1,2</sup> T.P. Estyunina,<sup>1</sup>  
A.V. Eryzhenkov,<sup>1</sup> K.A. Kokh,<sup>1,3</sup> O.E. Tereshchenko,<sup>1,4</sup> T. Iwata,<sup>5,6</sup> K. Kuroda,<sup>5,6,7</sup>  
K. Miyamoto,<sup>8</sup> T. Okuda,<sup>6,7,8</sup> K. Shimada,<sup>5,6,7,8</sup> and A.V. Tarasov<sup>1</sup>

<sup>1</sup>*Saint Petersburg State University, 198504 Saint Petersburg, Russia*

<sup>2</sup>*Institute of Molecule and Crystal Physics, Subdivision of the Ufa Federal Research Centre of the Russian Academy of Sciences, 450075 Ufa, Russia*

<sup>3</sup>*Sobolev Institute of Geology and Mineralogy, Siberian Branch, Russian Academy of Sciences, 630090 Novosibirsk, Russia*

<sup>4</sup>*Rzhanov Institute of Semiconductor Physics, Siberian Branch, Russian Academy of Sciences, 630090 Novosibirsk, Russia*

<sup>5</sup>*Graduate School of Advanced Science and Engineering, Hiroshima University, 739-8526 Higashi-Hiroshima, Japan*

<sup>6</sup>*International Institute for Sustainability with Knotted Chiral Meta Matter (WPI-SKCM<sup>2</sup>), Hiroshima University, 739-8526 Higashi-Hiroshima, Japan*

<sup>7</sup>*Research Institute for Semiconductor Engineering, Hiroshima University, 739-8527 Higashi-Hiroshima, Japan*

<sup>8</sup>*Research Institute for Synchrotron Radiation Science, Hiroshima University, 739-0046 Higashi-Hiroshima, Japan*

The spin-resolved dispersion dependencies for the topological insulator  $\text{Mn}_{1-x}\text{Ge}_x\text{Bi}_2\text{Te}_4$  in the  $\bar{K}\bar{\Gamma}\bar{K}'$  path of the Brillouin zone (BZ) were studied by spin- and angle-resolved photoemission spectroscopy using laser radiation (Laser Spin-ARPES) with variation of the concentration of substitutional Ge atoms ( $x$  from 0.1 to 0.8) for in-plane ( $s_x$ ) and out-of-plane ( $s_z$ ) spin orientation. The formation of Rashba-like states is shown, which shift to lower energies with increasing Ge concentration. In the region of Ge concentrations from 50% to 75%, the contribution of these states to the formed spin-dependent dispersions becomes predominant. A pronounced in-plane ( $s_y$ ) spin polarization, asymmetric for opposite  $\pm k_{\parallel}$  directions, is revealed for the Dirac cone states, while the Rashba-like states exhibit a pronounced asymmetry in both in-plane ( $s_y$ ) and out-of-plane ( $s_z$ ) spin polarizations. Theoretical calculations confirmed the asymmetric polarization of the Rashba-like states formed in the  $\bar{K}\bar{\Gamma}\bar{K}'$  path of the BZ, simultaneously for in-plane and out-of-plane spin orientation. Constant energy maps for Rashba-like states show a pronounced  $s_z$  spin component along the  $\bar{\Gamma}\bar{K}$  direction, with a sign change as the contour crosses the  $\bar{\Gamma}\bar{M}$  direction. The observed spin polarization can influence the development of spin devices based on magnetic topological insulators.

## I. INTRODUCTION

The interplay of magnetism and band topology in magnetic topological insulators (TIs) leads to many exotic quantum phenomena, for example, quantized anomalous Hall effect (QAHE), topological magnetoelectric effect (TME) and other unique topological properties [1–6]. Intrinsic magnetic topological insulators are a class of materials where magnetic atoms have definite crystallographic positions, the most notable representative being  $\text{MnBi}_2\text{Te}_4$  which was synthesized and experimentally studied several years ago [7–10]. Since magnetic atoms are arranged regularly, quantum topological effects such as QAHE can be observed at significantly higher temperatures, for example, QAHE is reachable in  $\text{MnBi}_2\text{Te}_4$  thin films at 1.4 K without any external magnetic field or at 6.5 K when such field is applied [11].

$\text{MnBi}_2\text{Te}_4$  is an antiferromagnetic (AFM) TI with a Néel temperature of approximately 24–25 K [7–11]. Experimental studies of its surface electronic structure revealed an anomalously large energy gap up to 90 meV

[7–17] in its topological surface states (TSS) which, however, exhibits such significant variations that even a gapless surface spectrum may be observed [18–20]. Numerous theoretical studies of  $\text{MnBi}_2\text{Te}_4$ -family materials reveal their band structures to be particularly sensitive to slight modifications of their geometry (e.g. first van der Waals gap magnitude), local atomic composition (lower- $Z$  dopants of magnetic moments or nonmagnetic doping of the magnetic layers) or other factors which influence TSS localization depth relative to the crystal surface [13–17, 21–25].

Such sensitive TSS behavior suggests that topological phase transitions (TPTs) may be driven externally in these materials [13–17]. It is hypothesized that even an axion-like state with its corresponding TME effect may be observed near the TPT point [17], which can be driven by application of an external electric field [24, 25]. Another possibility to influence the TPT can be a doping the Mn layer with atoms of IV group such as Ge, Sn or Pb [26–32]. The resulting materials have the  $\text{Mn}_{1-x}\text{A}_x\text{Bi}_2\text{Te}_4$  stoichiometry ( $A = \text{Ge}, \text{Sn}, \text{Pb}$ ) where TPTs are likely to occur for  $x \approx 40\% \dots 50\%$  [26–28], even a Weyl semimetal state is suggested for certain combinations of magnetic and atomic structures [33]. Char-

\* ashikin@inbox.ru

acteristic Néel temperatures and spin-flop transition field threshold for these compounds decrease from 24.5 K and 7 T in pristine  $\text{MnBi}_2\text{Te}_4$  to 10...15 K and 1...1.5 T, respectively, when  $x$  reaches  $\approx 50\% \dots 80\%$ ; further doping leads to values of 5 K and 0.5 T, respectively [34].

Due to the unique spin-momentum locked spin structure and corresponding charge-spin interconversion effects, magnetic TIs (including the  $\text{MnBi}_2\text{Te}_4$  family [14]) are now increasingly being used in spintronics [35]. For instance, the injection of an electric current into a TI is known to generate in-plane spin-transfer torques (STTs) orders of magnitude larger than in other materials with high spin-orbit coupling (SOC) strength [36]. These giant STTs are suitable for low-power current-induced magnetization switching in heterostructures consisting of a TI with a ferromagnetic (FM) layer.

Moreover, the design of topological insulators with out-of-plane surface spin texture could further expand the range of spintronic effects and related applications [37, 38]. For example, the current-induced magnetization of layers with perpendicular magnetic anisotropy, which are typically used in logic and memory devices, is switched more efficiently using the out-of-plane STTs instead of in-plane STTs [39].

In this study we explore Ge concentration-dependent in-plane and out-of-plane spin structure of  $\text{Mn}_{1-x}\text{Ge}_x\text{Bi}_2\text{Te}_4$  experimentally (through Laser Spin ARPES) and theoretically (using density functional theory (DFT) calculations), examining the underlying mechanisms driving the features of spin structure and their evolution.

## II. RESULTS OF EXPERIMENTAL MEASUREMENTS

Spin-resolved ARPES measurements of  $\text{Mn}_{1-x}\text{Ge}_x\text{Bi}_2\text{Te}_4$  for Ge concentration values  $x$  of 10%, 35%, 45%, 55% and 80% were performed using  $s$ -polarized laser radiation with photon energy  $h\nu = 6.3$  eV for both in-plane (Fig. 1) and out-of-plane (Fig. 2) spin polarizations. Fig. 1(b) and Fig. 2(a) show spin-resolved data with Sherman function corrections for spin-up ( $I_\uparrow$ , red) and spin-down ( $I_\downarrow$ , blue) orientations. Fig. 1(c) and Fig. 2(b) present the normalized maximal intensity differences  $I_\uparrow - I_\downarrow$ , while Fig. 1(d) and Fig. 2(c) show spin polarization diagrams calculated as  $\frac{I_\uparrow - I_\downarrow}{I_\uparrow + I_\downarrow}$ . Experimental band structures without spin resolution are shown in Fig. 1(a) as a reference for assessing band structure evolution with increasing Ge concentration, similar to earlier works [27, 33].

*Spin-integrated band structure.* At 10% doping, the band structure in Fig. 1(a1) shows typical TSS Dirac cone structure with Dirac point (DP) position located at the energy of 0.22 eV. Valence and conduction band (VB and CB) edges are observed at the energy of 0.30 eV and 0.15 eV, respectively. A feature marked Q appears near the Fermi level (FL) with further development at higher

Ge-concentrations (it is more visible in spin-resolved dispersion).

With increasing Ge concentration, a new feature (marked R) appears in the CB energy region, attributed to Rashba-like states with surface character [33]. These states evolve with Ge doping and are Ge-contributed. At 35% Ge and then at 45% Ge (Fig. 1(a2, a3)), Rashba-like states coexist with the Dirac cone, but further concentration increase makes original TSS indistinguishable whereas these Rashba-like states shift in energy and become a prevalent band structure feature along with gapless bulk states. At 55% Ge (Fig. 1(a4)), Rashba-like states form two distinct parabolic branches split by CB states at the  $\Gamma$  point. The outer branches of these states (feature R) shift to lower energies as  $x$  increases, reaching the energy of 0.25 eV at 80% Ge (Fig. 1(a5)), surpassing the original DP position. At such high concentrations, the bulk band gap reopens, and the band structure resembles Mn-doped  $\text{GeBi}_2\text{Te}_4$ . Similar Rashba-like states have been previously observed in  $\text{Mn}_{1-x}\text{Ge}_x\text{Bi}_2\text{Te}_4$  and  $\text{Mn}_{1-x}\text{Sn}_x\text{Bi}_2\text{Te}_4$  systems [26, 27, 33], suggesting that the energy shifts observed in our measurements may be a common feature across these materials.

*Spin-resolved band structure.* Spin-resolved ARPES reveals detailed band structure features. At 10% doping, the in-plane spin structure of the Dirac cone shows typical spin-momentum locking for helical TSS in topological insulators, as seen in Fig. 1(d1). The in-plane spin polarization reverses ( $I_\uparrow \longleftrightarrow I_\downarrow$ ) together with planar electron quasimomentum ( $-k_\parallel \longleftrightarrow +k_\parallel$ ).

The studied system with Ge concentration of 35% has a very similar in-plane spin structure in Fig. 1(b2—d2) which exhibits in-plane spin reversal when the planar quasimomentum  $k_\parallel$  is reversed. In particular, the left branches of both features R (Rashba-like states) and Q are positively polarized ( $I_\uparrow$ ). The out-of-plane spin structure becomes more noticeable in Fig. 2(c2), where the lower Dirac cone part acquires detectable out-of-plane polarization ( $I_\uparrow$  for left branch,  $I_\downarrow$  for right branch). The above-mentioned Rashba-like states with opposite out-of-plane polarizations begin to manifest themselves already at 35% Ge near the Fermi level (marked as R states with corresponding arrows), see Fig. 2(b2).

At 45% and higher Ge concentrations, the spin polarization of feature Q is reversed at the same time when parabolic branches of Rashba-like states (R) become pronounced. This supports the idea that feature Q is a continuation of the branches of the Rashba-like states. Both in-plane and out-of-plane polarizations of feature R intensify with increasing Ge content, while feature Q shows also the out-of-plane polarization. At higher Ge concentrations ( $x = 80\%$ ) the Rashba-like states still exhibit their pronounced character.

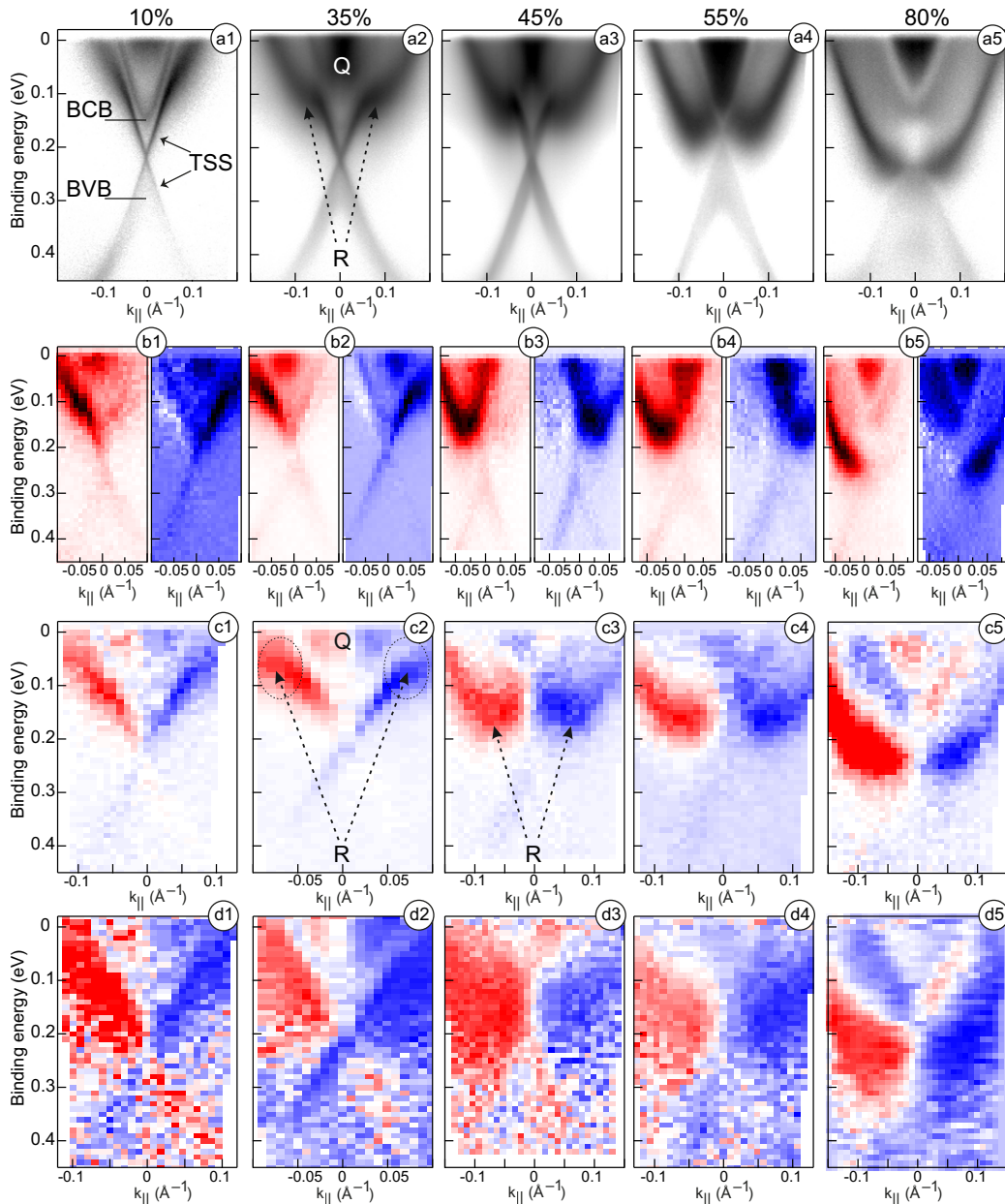


FIG. 1. **(a1–a5)** Experimental spin-integrated ARPES data for  $\text{Mn}_{1-x}\text{Ge}_x\text{Bi}_2\text{Te}_4$  with different  $x$  measured using  $s$ -polarized laser radiation with photon energy  $h\nu = 6.3$  eV. **(b1–b5)** Experimental spin-resolved ARPES data for in-plane spin polarization with opposite spin orientations ( $I_\uparrow$  in red,  $I_\downarrow$  in blue) reconstructed using the Sherman function. **(c1–c5)** Intensity-normalized maps of spin polarization difference ( $I_\uparrow - I_\downarrow$ ) where dominant polarizations are color-coded according to the panel (b). **(d1–d5)** Conventional spin polarization maps calculated from raw data by the formula  $(I_\uparrow - I_\downarrow)/(I_\uparrow + I_\downarrow)$ .

### III. RESULTS OF THEORETICAL CALCULATIONS

In order to understand the band and spin structure of  $\text{Mn}_{1-x}\text{Ge}_x\text{Bi}_2\text{Te}_4$ , a DFT computational study was performed on supercells to simulate Ge doping (see Methods for details). Fig. 3 shows the calculated band structures for Ge concentrations of 25%, 33%, 50%, 66%, and 75% along the  $\bar{\Gamma}\bar{K}$  direction ( $x$  axis). Panel 3(a) illustrates

spatial localizations of the states, while panels 3(b) and 3(c) show  $s_y$  (in-plane, perpendicular to the Brillouin zone path) and  $s_z$  (out-of-plane) spin polarizations, respectively.

According to the obtained results, the calculated bands display behavior very similar to the experimental data. Increasing Ge concentration leads to the formation of Rashba-like states (features R and Q) with significant in-plane (up to 50%, see panels 3(b,d)) and out-of-plane

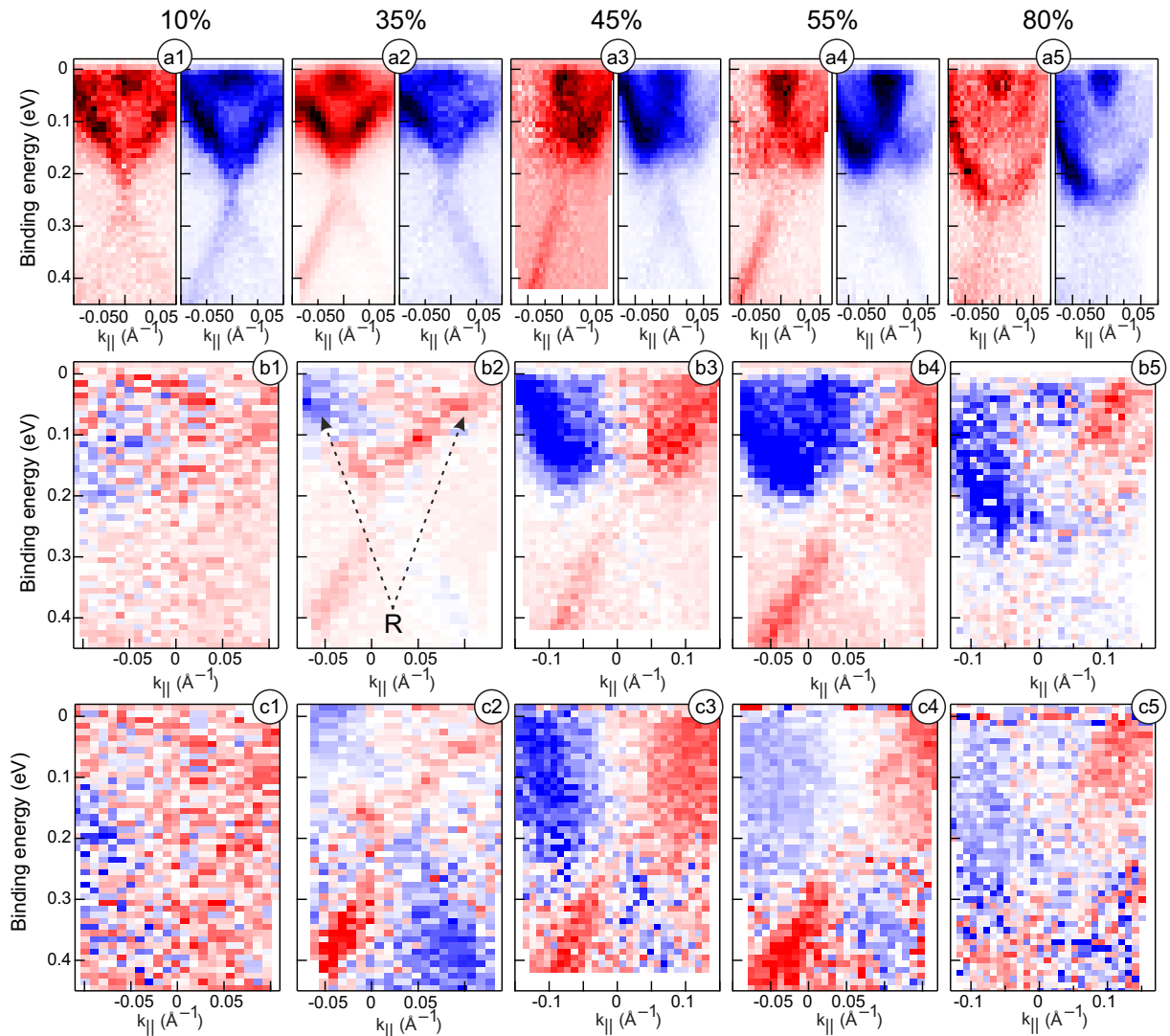


FIG. 2. **(a1–a5)** Experimental spin-resolved ARPES data for out-of-plane spin polarization with opposite spin orientations ( $I_{\uparrow}$  in red,  $I_{\downarrow}$  in blue) reconstructed using the Sherman function. **(b1–b5)** Intensity-normalized maps of spin polarization difference ( $I_{\uparrow} - I_{\downarrow}$ ) where dominant polarizations are color-coded according to the panel (a). **(c1–c5)** Conventional spin polarization maps calculated from raw data by the formula  $(I_{\uparrow} - I_{\downarrow})/(I_{\uparrow} + I_{\downarrow})$ .

spin polarizations (up to 15%, see panels 3(c,d)). These states (R) become more pronounced and shift to lower energies, consistent with previous DFT studies of similar systems doped with Ge or Sn [26, 27, 33].

Moreover, these Rashba-like states are almost completely localized at the surface in the first SL (see panel 3(a)) for all Ge concentrations, while the TSS, which exist at low Ge concentrations, diffuse deeper into the bulk. Notably, at  $x = 25\%$ , the upper Dirac cone band already shows strong surface localization in the energy range  $+0.2 \dots 0.3$  eV (see Fig. 3(a1)), where the Rashba-like states begin to form as Ge doping increases.

Fig. 3(d1–d6) shows spin profiles for Ge concentrations of 25%, 50%, and 75% along the vertical dashed lines  $k_{\parallel} = \pm 0.12 \text{ \AA}^{-1}$ , illustrating the in-plane and out-of-plane spin polarizations of the intersected states (mostly

the outer branches of the Rashba-like states). It is clearly observed that the out-of-plane polarization is actually much weaker than the in-plane polarization.

*In-plane spin structure.* At 25% Ge the band structure shows spin-momentum locking typical for TSS (Fig. 3(b1)) while another band located at  $+0.25$  eV displays similar behavior. This band likely represents feature Q from the experimental spectra in Fig. 1(a1–d1). As Ge concentration increases, the TSS disappear ( $x = 50\%$ ), with bands below the DP losing in-plane spin polarization and the Rashba-like states above the DP gaining it. By 66% Ge, the parabolic Rashba-like bands become pronounced, and features R and Q shift down in energy, consistent with experimental results (Fig. 1(c3–c5)).

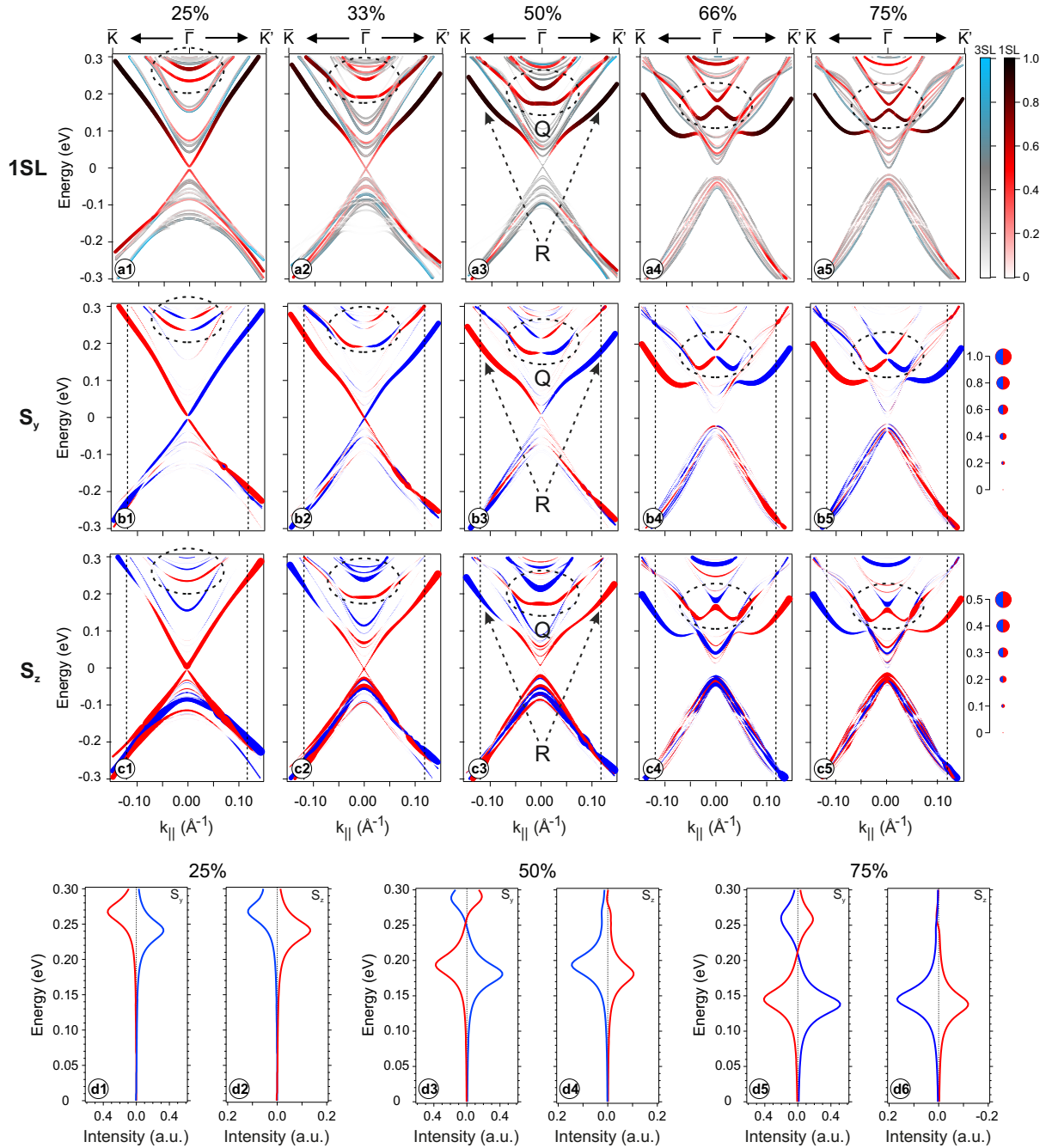


FIG. 3. **(a1–a5)** Calculated band structure of 12 SL thick slab of  $\text{Mn}_{1-x}\text{Ge}_x\text{Bi}_2\text{Te}_4$  along the  $\bar{\Gamma}\bar{K}$  direction ( $x$ ) in the BZ for Ge concentrations from 25% to 75% with distinguished the first (white-red-black) and third (gray-blue) SLs contributions, color intensity defines the localization degree. **(b1–b5)** and **(c1–c5)** depict in-plane  $s_y$  and out-of-plane  $s_z$  spin polarizations, respectively. Positive and negative spin polarizations along the corresponding directions are shown by red and blue symbols, where symbol sizes determine the spin polarization magnitudes. **(d1–d6)** Spin distribution profiles for  $x$  values of 25%, 50% and 75% taken along vertical dashed lines at  $k_{\parallel} = \pm 0.12 \text{ \AA}^{-1}$  for bands with  $s_y$  and  $s_z$  spin polarizations.

*Out-of-plane spin structure.* Fig. 3(c) shows three notable observations. First, at low Ge concentrations, spin-polarized features appear at +0.25 eV (which later form the Rashba-like states), as also seen in the experimental data (Fig. 2(b2)). At  $x = 66\%$  and 75%, well-defined

Rashba-like states are formed, with out-of-plane spin polarization also inverted relative to the  $\Gamma$  point. Only the outer branches of the Rashba-like states (feature R) show out-of-plane spin inversion with  $k_{\parallel}$  reversal, clearly seen experimentally in Fig. 2(b3, b4). In these outer branches,

both red and blue regions are present, indicating opposite spin projections for different states as the wave vector  $k_{\parallel}$  increases. The feature Q and other states show consistent polarization regardless of quasimomentum direction, as confirmed by experimental features near the FL (Fig. 2(a4–a5)).

Further exploration of the non-trivial out-of-plane spin texture is possible through out-of-plane spin-polarized constant energy contours in the  $k_x$ – $k_y$  plane. These contours, shown in Fig. 4, depict systems with  $x = 50\%$  and  $75\%$ . The constant energy contours taken far from the  $\Gamma$  point exhibit a trigonal spin texture, with the out-of-plane spin polarization alternating every  $60^\circ$  with maxima in the  $\bar{\Gamma}\bar{K}$  direction and reaching zero at the  $\bar{\Gamma}\bar{M}$  direction. However, the images lack threefold rotation symmetry due to broken inversion symmetry (Fig. 4(a4)), where the contour closer to  $\Gamma$  shows positive out-of-plane spin polarization but is not perfectly circular.

As a result, it can be stated that both experimental data and DFT calculations for  $\text{Mn}_{1-x}\text{Ge}_x\text{Bi}_2\text{Te}_4$  confirm existence of surface states with parabolic-like outer branches with helical in-plane spin texture as well as non-trivial out-of-plane spin texture. In-plane helicity together with predominant surface localization suggest strong resemblance of these states to those which occur in the canonical Rashba effect with two-dimensional electron gas [40–42], hence the term “Rashba-like states” used throughout this paper.

#### IV. DISCUSSION

Contrary to the simplest interpretation of the Rashba model [40, 42–44], in our case, the formation of Rashba-like spin-momentum locking states can be associated with the asymmetric hybridization of  $p_{x(y)}$  and  $p_z$  orbitals, mediated by  $s$  orbitals, under interaction of Ge atoms (replacing Mn atoms) with Te and Bi atoms in the nearest layers. This leads to the formation of a  $\mathbf{k}$ -antisymmetric momentum-dependent orbital momentum  $\mathbf{L}_n(\mathbf{k}) = -\mathbf{L}_n(-\mathbf{k})$ , resulting from inversion symmetry breaking [41]. This orbital momentum couples to the spin in the presence of spin-orbit coupling, forming Rashba-like spin-momentum locking [41, 45, 46]. The formation of such states depends on chemical bonds, making them Ge-contributed and shifting in energy with changing Ge concentration. The influence of this orbital momentum is strongest near the nucleus [41, 42, 45], where spin-orbit coupling is most effective. The inclusion of Ge  $p$  states (instead of Mn  $sd$  states) enhances Rashba-like effects, since  $p$ -electrons approach the nucleus more closely than  $d$ -electrons [41, 42]. As a result, Rashba-like effects in systems based on  $p$ -electrons, such as Ge-doped materials, are more pronounced, with the inversion symmetry breaking at the surface leading to surface Rashba states, similar to classical Rashba effects.

The formation of Rashba-like states with out-of-plane spin polarization ( $s_z$ ) was also observed in Bi/Ag systems

[43, 44, 47]. In [48], it was shown that for Bi/Ag(111) and Pb/Ag(111), an out-of-plane spin component ( $s_z$ ) accompanies in-plane polarization ( $s_{x,y}$ ) due to partial spin rotation between the K and M points of the surface BZ. This component is maximal along  $\bar{\Gamma}\bar{K}$  and minimal along  $\bar{\Gamma}\bar{M}$ .

Similar effects of spin polarization transformation between  $s_{x,y}$  and  $s_z$  are seen in topological surface states (TSS) of topological insulators near the Fermi level due to warping effects [49–52]. These effects, which create an out-of-plane spin component along  $\bar{\Gamma}\bar{K}$  while preserving in-plane polarization along  $\bar{\Gamma}\bar{M}$ , are strongest near the Fermi level and minimal near the Dirac point.

For the systems in this work, inversion symmetry breaking in the  $\bar{\Gamma}\bar{K}$  direction plays a significant role. Similar effects were observed in Refs [7, 53, 54] for systems based on  $\text{MnBi}_2\text{Te}_4$ ,  $\text{GeBi}_2\text{Te}_4$ ,  $\text{MnBi}_2\text{Te}_4/\text{Bi}_2\text{Te}_3$  as well as Bi/ $\text{MnBi}_2\text{Te}_4$  and Bi/ $\text{Bi}_2\text{Se}_3$  bilayers [55, 56], where asymmetry in the  $\bar{\Gamma}\bar{K}$  direction was linked to crystal symmetry and the interplay of spin-orbit coupling and exchange fields. As a result, the right and left branches of states interact with the Zeeman field in different ways, leading to a difference in the left and right branches of states ( $E(+k)$  is not equal to  $E(-k)$ ) and the formation of the  $s_z$  spin component in the  $\bar{K}\bar{\Gamma}\bar{K}'$  path, which coexists with the in-plane  $s_{x,y}$  polarizations. Time-reversal and inversion symmetry breaking cause  $E(+k) \neq E(-k)$ , leading to an  $s_z$  spin component in the  $\bar{\Gamma}\bar{K}$  direction along with in-plane polarization [7, 53, 54]. This results in a threefold, rather than sixfold, momentum inversion asymmetry.

In contrast, along the  $\bar{\Gamma}\bar{M}$  direction, the (0001) surface of  $\text{MnBi}_2\text{Te}_4$  has three mirror planes, maintaining symmetry along  $\bar{\Gamma}\bar{M}$ , which suppresses inversion asymmetry and causes the  $s_z$  component to approach zero in this direction [7, 53, 54].

To confirm this, Fig. 4 presents constant energy contours including out-of-plane spin component for systems with 50% and 75% Ge concentrations. Spin-resolved dispersion dependencies in the  $\bar{\Gamma}\bar{K}$  and  $\bar{\Gamma}\bar{M}$  directions for energies above the DP are also shown which indicate the contour energy levels by horizontal dotted lines. The contours taken at energies between 0.1 and 0.2 eV show threefold symmetry with spin inversion in the  $\pm k_{\parallel}$  Rashba-like branches along the  $\bar{K}\bar{\Gamma}\bar{K}'$  direction. This correlates with the dispersion calculations (Fig. 3) and experimentally measured dispersions (Figs 1, 2). Contours taken near 0.08–0.09 eV correspond to the Dirac cone states and represent distorted circles without apparent spin orientation changes in agreement with Fig. 3. Along the  $\bar{\Gamma}\bar{M}$  direction, the spin inversion changes sign and  $s_z$  component vanishes.

Thus, both experimental and theoretical results show good agreement for spin orientations in the  $\bar{\Gamma}\bar{K}$  direction, confirming the analysis of the observed phenomena.

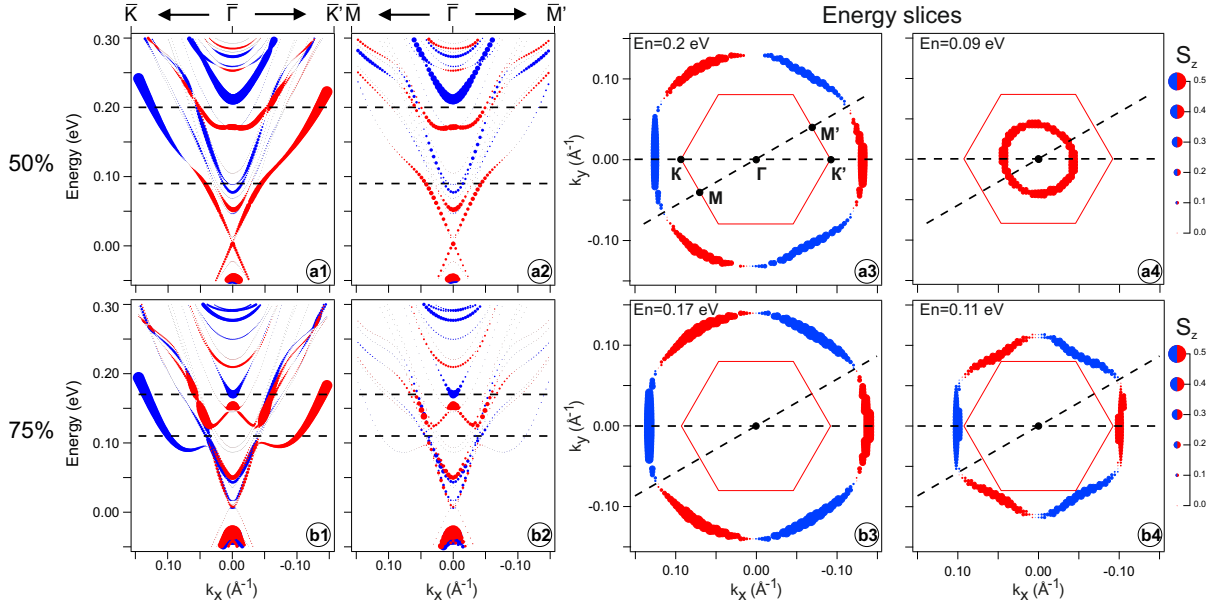


FIG. 4. Constant energy contours for outer branches of the Rashba-like states with out-of-plane spin polarization for  $\text{Mn}_{1-x}\text{Ge}_x\text{Bi}_2\text{Te}_4$  with 50% and 75% Ge concentrations. Spin-resolved dispersions along the  $\bar{\Gamma}\bar{K}$  and  $\bar{\Gamma}\bar{M}$  directions together with out-of-plane spin polarization are provided for reference; the corresponding energy levels are shown with dashed lines. Each energy contour is provided together with a hexagonal image of the Brillouin zone (not to scale) which displays alignment of principal symmetry directions.

## V. METHODS

First-principles calculations in the framework of the density functional theory (DFT) were performed at the Computing Center of SPbU Research park. The electronic structure supercell calculations with impurities were performed using the OpenMX DFT code which implements a linear combination of pseudo-atomic orbitals (LCPAO) approach [57–59] with full-relativistic norm-conserving pseudopotentials [60]. The GGA-PBE exchange-correlation pseudopotential [61] was utilized and basis sets were specified as Ge7.0-s3p2d2, Mn6.0-s3p2d1, Te7.0-s3p2d2f1 and Bi8.0-s3p2d2f1 where numbers mean interaction ranges in Å. Real-space numerical integration accuracy was specified by cutoff energy of 200 Ry, total energy convergence criterion was  $2 \times 10^{-5}$  Hartree. The Mn  $3d$  states were considered within the DFT +  $U$  approach [62] with  $U = 5.4$  eV.

Simulation of  $\text{Mn}_{1-x}\text{Ge}_x\text{Bi}_2\text{Te}_4$  compounds for  $x$  values of 25%, 50% and 75% was performed using  $2 \times 2$  supercells whereas  $3 \times 1$  supercells were used for Ge concentrations of 33% and 66%. Surface band structures were calculated for 12 SL slabs separated by 20 Å vacuum gaps in the  $z$  direction (the surface normal) while constant energy contours were calculated using 6 SL slab thickness. Surface Brillouin zones of  $2 \times 2$  ( $3 \times 1$ ) supercells were sampled with regular  $3 \times 3$  ( $3 \times 5$ ) meshes of  $\mathbf{k}$ -points, respectively.

Spin-resolved APRES experiments were performed with LaserSpin ARPES station with Scienta DA30 analyzer stationed at HiSOR [63] (Hiroshima, Japan) with

photon energy of  $h\nu = 6.3$  eV was used. All measurements were conducted under ultra-high vacuum conditions (base pressure was less than  $10 \times 10^{-10}$  Torr) and sample temperatures below 30 K. Stoichiometric compositions of analyzed samples were estimated using X-ray photoelectron spectroscopy (XPS) with Al  $K_\alpha$  ( $h\nu = 1486.7$  eV) radiation.

## VI. CONCLUSION

Experimental and theoretical studies of the spin electron structure with in-plane and out-of-plane spin orientation for TI  $\text{Mn}_{1-x}\text{Ge}_x\text{Bi}_2\text{Te}_4$  with a change in the concentration of substituting Ge atoms are carried out. The formation of Ge-contributed Rashba-like states is shown, characterized in addition to the bulk-derived origin also by a significant surface contribution, which shift to lower energies as the Ge concentration increases. These states determine the main contribution to the formed structure of  $\text{Mn}_{1-x}\text{Ge}_x\text{Bi}_2\text{Te}_4$ .

Experimental studies and theoretical calculations have shown that these Rashba-like states are characterized by pronounced in-plane and out-of-plane spin polarizations along the  $\bar{\Gamma}\bar{K}$  direction of the BZ, with inversion in the  $\pm k_{\parallel}$  directions relative to the  $\Gamma$  point. Overall, a strong correlation is observed between the experimentally measured spin-resolved dispersion relations and the corresponding theoretical calculations. Theoretical studies of constant energy maps for Rashba-like states also show that the sign of the  $s_z$  spin component changes as the

contour crosses the  $\bar{\Gamma M}$  direction.

The observed spin polarization, especially the distinct in-plane and out-of-plane spin textures of the Rashba-like states, opens up new opportunities for the development of advanced spintronic devices. The strong spin-momentum locking and the ability to control spin orientation via Ge doping make  $\text{Mn}_{1-x}\text{Ge}_x\text{Bi}_2\text{Te}_4$  a promising candidate for applications in low-power spintronic technologies, such as spin transistors and memory devices. Additionally, the tunable nature of the Rashba-like states and their surface localization could be exploited in the design of heterostructures, enabling efficient spin-charge interconversion and current-induced magnetization switching. These properties position  $\text{Mn}_{1-x}\text{Ge}_x\text{Bi}_2\text{Te}_4$  as a versatile material platform for future magnetic topological insulator-based spintronic applications.

### ACKNOWLEDGMENTS

This work was supported by the Russian Science Foundation grant No. 23-12-00016 and the St. Petersburg State University grant No. 95442847.

HiSOR ARPES measurements were performed under Proposals No. 23AU012 and 23BU003. We are grateful to the N-BARD, Hiroshima University for liquid He supplies. The calculations were partially performed using the equipment of the Joint Supercomputer Center of the Russian Academy of Sciences (<https://rscgroup.ru/en/project/jscc>). Monocrystalline  $\text{Mn}_{1-x}\text{Ge}_x\text{Bi}_2\text{Te}_4$  samples were grown using the Bridgman method under the state assignment of Sobolev Institute of Geology and Mineralogy SB RAS No. 122041400031-2.

- 
- [1] X.-L. Qi, T. L. Hughes, and S.-C. Zhang, Topological field theory of time-reversal invariant insulators, *Physical Review B* **78**, 195424 (2008).
- [2] X.-L. Qi and S.-C. Zhang, Topological insulators and superconductors, *Reviews of modern physics* **83**, 1057 (2011).
- [3] Y. Tokura, K. Yasuda, and A. Tsukazaki, Magnetic topological insulators, *Nature Reviews Physics* **1**, 126 (2019).
- [4] C.-Z. Chang, C.-X. Liu, and A. H. MacDonald, Colloquium: Quantum anomalous Hall effect, *Reviews of Modern Physics* **95**, 011002 (2023).
- [5] C.-Z. Chang, J. Zhang, X. Feng, J. Shen, Z. Zhang, M. Guo, K. Li, Y. Ou, P. Wei, L.-L. Wang, *et al.*, Experimental observation of the quantum anomalous Hall effect in a magnetic topological insulator, *Science* **340**, 167 (2013).
- [6] P. Wang, J. Ge, J. Li, Y. Liu, Y. Xu, and J. Wang, Intrinsic magnetic topological insulators, *The Innovation* **2** (2021).
- [7] M. M. Otrokov, I. I. Klimovskikh, H. Bentmann, D. Estyunin, A. Zeugner, Z. S. Aliev, S. Gaß, A. Wolter, A. Koroleva, A. M. Shikin, *et al.*, Prediction and observation of an antiferromagnetic topological insulator, *Nature* **576**, 416 (2019).
- [8] J. Li, Y. Li, S. Du, Z. Wang, B.-L. Gu, S.-C. Zhang, K. He, W. Duan, and Y. Xu, Intrinsic magnetic topological insulators in van der Waals layered  $\text{MnBi}_2\text{Te}_4$ -family materials, *Science Advances* **5**, eaaw5685 (2019).
- [9] D. Zhang, M. Shi, T. Zhu, D. Xing, H. Zhang, and J. Wang, Topological axion states in the magnetic insulator  $\text{MnBi}_2\text{Te}_4$  with the quantized magnetoelectric effect, *Physical Review Letters* **122**, 206401 (2019).
- [10] Y. Gong, J. Guo, J. Li, K. Zhu, M. Liao, X. Liu, Q. Zhang, L. Gu, L. Tang, X. Feng, *et al.*, Experimental realization of an intrinsic magnetic topological insulator, *Chinese Physics Letters* **36**, 076801 (2019).
- [11] Y. Deng, Y. Yu, M. Z. Shi, Z. Guo, Z. Xu, J. Wang, X. H. Chen, and Y. Zhang, Quantum anomalous Hall effect in intrinsic magnetic topological insulator  $\text{MnBi}_2\text{Te}_4$ , *Science* **367**, 895 (2020).
- [12] D. Estyunin, I. I. Klimovskikh, A. M. Shikin, E. Schvier, M. Otrokov, A. Kimura, S. Kumar, S. Filnov, Z. S. Aliev, M. Babanly, *et al.*, Signatures of temperature driven antiferromagnetic transition in the electronic structure of topological insulator  $\text{MnBi}_2\text{Te}_4$ , *APL Materials* **8**, 021105 (2020).
- [13] A. M. Shikin, D. A. Estyunin, N. L. Zaitsev, D. Glazkova, I. I. Klimovskikh, S. O. Filnov, A. G. Rybkin, E. F. Schvier, S. Kumar, A. Kimura, N. Mamedov, Z. Aliev, M. B. Babanly, K. Kokh, O. E. Tereshchenko, M. M. Otrokov, E. V. Chulkov, K. A. Zvezdin, and A. K. Zvezdin, Sample-dependent Dirac-point gap in  $\text{MnBi}_2\text{Te}_4$  and its response to applied surface charge: A combined photoemission and *ab initio* study, *Physical Review B* **104**, 115168 (2021).
- [14] A. M. Shikin, D. Estyunin, I. I. Klimovskikh, S. Filnov, E. Schvier, S. Kumar, K. Miyamoto, T. Okuda, A. Kimura, K. Kuroda, *et al.*, Nature of the Dirac gap modulation and surface magnetic interaction in axion antiferromagnetic topological insulator  $\text{MnBi}_2\text{Te}_4$ , *Scientific Reports* **10**, 13226 (2020).
- [15] A. Shikin, T. Makarova, A. Eryzhenkov, D. Y. Usachov, D. Estyunin, D. Glazkova, I. Klimovskikh, A. Rybkin, and A. Tarasov, Routes for the topological surface state energy gap modulation in antiferromagnetic  $\text{MnBi}_2\text{Te}_4$ , *Physica B: Condensed Matter* **649**, 414443 (2023).
- [16] M. Garnica, M. M. Otrokov, P. C. Aguilar, I. I. Klimovskikh, D. Estyunin, Z. S. Aliev, I. R. Amiraslanov, N. A. Abdullayev, V. N. Zverev, M. B. Babanly, *et al.*, Native point defects and their implications for the Dirac

- point gap at  $\text{MnBi}_2\text{Te}_4$  (0001), *npj Quantum Materials* **7**, 7 (2022).
- [17] A. Shikin, T. Estyunina, A. Eryzhenkov, N. Zaitsev, and A. Tarasov, Topological phase transition in the antiferromagnetic topological insulator  $\text{MnBi}_2\text{Te}_4$  from the point of view of axion-like state realization, *Scientific Reports* **13**, 16343 (2023).
- [18] Y.-J. Hao, P. Liu, Y. Feng, X.-M. Ma, E. F. Schwier, M. Arita, S. Kumar, C. Hu, R. Lu, M. Zeng, *et al.*, Gapless surface Dirac cone in antiferromagnetic topological insulator  $\text{MnBi}_2\text{Te}_4$ , *Physical Review X* **9**, 041038 (2019).
- [19] Y. J. Chen, L. X. Xu, J. H. Li, Y. W. Li, H. Y. Wang, C. F. Zhang, H. Li, Y. Wu, A. J. Liang, C. Chen, S. W. Jung, C. Cacho, Y. H. Mao, S. Liu, M. X. Wang, Y. F. Guo, Y. Xu, Z. K. Liu, L. X. Yang, and Y. L. Chen, Topological electronic structure and its temperature evolution in antiferromagnetic topological insulator  $\text{MnBi}_2\text{Te}_4$ , *Physical Review X* **9**, 041040 (2019).
- [20] P. Swatek, Y. Wu, L.-L. Wang, K. Lee, B. Schruck, J. Yan, and A. Kaminski, Gapless Dirac surface states in the antiferromagnetic topological insulator  $\text{MnBi}_2\text{Te}_4$ , *Physical Review B* **101**, 161109(R) (2020).
- [21] S. Chowdhury, K. F. Garrity, and F. Tavazza, Prediction of Weyl semimetal and antiferromagnetic topological insulator phases in  $\text{Bi}_2\text{MnSe}_4$ , *npj Computational Materials* **5**, 33 (2019).
- [22] H. Zhang, W. Yang, Y. Wang, and X. Xu, Tunable topological states in layered magnetic materials of  $\text{MnSb}_2\text{Te}_4$ ,  $\text{MnBi}_2\text{Se}_4$ , and  $\text{MnSb}_2\text{Se}_4$ , *Physical Review B* **103**, 094433 (2021).
- [23] L. Zhou, Z. Tan, D. Yan, Z. Fang, Y. Shi, and H. Weng, Topological phase transition in the layered magnetic compound  $\text{MnSb}_2\text{Te}_4$ : Spin-orbit coupling and interlayer coupling dependence, *Physical Review B* **102**, 085114 (2020).
- [24] A. Shikin, D. Estyunin, N. Zaitsev, D. Glazkova, I. Klimovskikh, S. Fil'nov, A. Rybkin, K. Kokh, O. Tereshchenko, K. Zvezdin, *et al.*, Modulation of the Dirac point band gap in the antiferromagnetic topological insulator  $\text{MnBi}_2\text{Te}_4$  due to the surface potential gradient change, *Journal of Experimental and Theoretical Physics* **134**, 103 (2022).
- [25] A. Shikin, T. Estyunina, E. AV, N. Zaitsev, and A. Tarasov, Study of the relationship between topological phase transition, axion-like state, and magnetoelectric effect in an antiferromagnetic topological insulator  $\text{MnBi}_2\text{Te}_4$ , *JETP (russian)* **165**, 544 (2024).
- [26] A. V. Tarasov, T. P. Makarova, D. A. Estyunin, A. V. Eryzhenkov, I. I. Klimovskikh, V. A. Golyashov, K. A. Kokh, O. E. Tereshchenko, and A. M. Shikin, Topological phase transitions driven by Sn doping in  $\text{Mn}_{1-x}\text{Sn}_x\text{Bi}_2\text{Te}_4$ , *Symmetry* **15**, 469 (2023).
- [27] T. P. Estyunina, A. M. Shikin, D. A. Estyunin, A. V. Eryzhenkov, I. I. Klimovskikh, K. A. Bokai, V. A. Golyashov, K. A. Kokh, O. E. Tereshchenko, S. Kumar, *et al.*, Evolution of  $\text{Mn}_{1-x}\text{Ge}_x\text{Bi}_2\text{Te}_4$  electronic structure under variation of Ge content, *Nanomaterials* **13**, 2151 (2023).
- [28] A. S. Frolov, D. Y. Usachov, A. V. Tarasov, A. V. Fedorov, K. A. Bokai, I. Klimovskikh, V. S. Stolyarov, A. I. Sergeev, A. N. Lavrov, V. A. Golyashov, *et al.*, Magnetic Dirac semimetal state of  $(\text{Mn}, \text{Ge})\text{Bi}_2\text{Te}_4$ , *Communications Physics* **7**, 180 (2024).
- [29] T. Qian, Y.-T. Yao, C. Hu, E. Feng, H. Cao, I. I. Mazin, T.-R. Chang, and N. Ni, Magnetic dilution effect and topological phase transitions in  $(\text{Mn}_{1-x}\text{Pb}_x)\text{Bi}_2\text{Te}_4$ , *Physical Review B* **106**, 045121 (2022).
- [30] S. Changdar, S. Ghosh, K. Vijay, I. Kar, S. Routh, P. Maheshwari, S. Ghorai, S. Banik, and S. Thirupathiah, Nonmagnetic Sn doping effect on the electronic and magnetic properties of antiferromagnetic topological insulator  $\text{MnBi}_2\text{Te}_4$ , *Physica B: Condensed Matter* **657**, 414799 (2023).
- [31] J. Zhu, M. Naveed, B. Chen, Y. Du, J. Guo, H. Xie, and F. Fei, Magnetic and electrical transport study of the antiferromagnetic topological insulator Sn-doped  $\text{MnBi}_2\text{Te}_4$ , *Physical Review B* **103**, 144407 (2021).
- [32] J. Yan, The elusive quantum anomalous Hall effect in  $\text{MnBi}_2\text{Te}_4$ : a materials perspective, arXiv preprint arXiv:2112.09070 (2021).
- [33] A. Shikin, N. Zaitsev, T. Estyunina, D. Estyunin, A. Rybkin, D. Glazkova, I. Klimovskikh, A. Eryzhenkov, K. Kokh, V. Golyashov, *et al.*, Phase transitions, Dirac and WSM states in  $(\text{Mn}_{1-x}\text{Ge}_x)\text{Bi}_2\text{Te}_4$ , *Scientific Reports* (2024).
- [34] D. A. Estyunin, A. A. Rybkina, K. A. Kokh, O. E. Tereshchenko, M. V. Likholetova, I. I. Klimovskikh, and A. M. Shikin, Comparative study of magnetic properties of  $(\text{Mn}_{1-x}\text{a}_x^{\text{IV}})\text{Bi}_2\text{Te}_4$  ( $\text{a}^{\text{IV}} = \text{Ge}, \text{Pb}, \text{Sn}$ ), *Magnetochemistry* **9**, 210 (2023).
- [35] S. Zhang and A. Fert, Conversion between spin and charge currents with topological insulators, *Physical Review B* **94**, 184423 (2016).
- [36] A. R. Mellnik, J. Lee, A. Richardella, J. L. Grab, P. J. Mintun, M. H. Fischer, A. Vaezi, A. Manchon, E.-A. Kim, N. Samarth, *et al.*, Spin-transfer torque generated by a topological insulator, *Nature* **511**, 449 (2014).
- [37] J. Han and L. Liu, Topological insulators for efficient spin-orbit torques, *APL Materials* **9** (2021).
- [38] Y. Liu and Q. Shao, Two-dimensional materials for energy-efficient spin-orbit torque devices, *ACS nano* **14**, 9389 (2020).
- [39] S. Ikeda, K. Miura, H. Yamamoto, K. Mizunuma, H. Gan, M. Endo, S. Kanai, J. Hayakawa, F. Matsukura, and H. Ohno, A perpendicular-anisotropy  $\text{CoFeB-MgO}$  magnetic tunnel junction, *Nature Materials* **9**, 721 (2010).
- [40] Y. Bychkov and É. Rashba, Properties of a 2d electron gas with lifted spectral degeneracy, *JETP Letters* **39**, 78 (1984).
- [41] G. Bihlmayer, P. Noël, D. V. Vyalikh, E. V. Chulkov, and A. Manchon, Rashba-like physics in condensed matter, *Nature Reviews Physics* **4**, 642 (2022).
- [42] E. Krasovskii, Spin-orbit coupling at surfaces and 2d materials, *Journal of Physics: Condensed Matter* **27**, 493001 (2015).
- [43] C. R. Ast, J. Henk, A. Ernst, L. Moreschini, M. C. Falub, D. Pacilé, P. Bruno, K. Kern, and M. Grioni, Giant spin splitting through surface alloying, *Physical Review Letters* **98**, 186807 (2007).
- [44] J. Prempfer, M. Trautmann, J. Henk, and P. Bruno, Spin-orbit splitting in an anisotropic two-dimensional electron gas, *Physical Review B—Condensed Matter and Materials Physics* **76**, 073310 (2007).
- [45] S. R. Park, C. H. Kim, J. Yu, J. H. Han, and C. Kim, Orbital-angular-momentum based origin of Rashba-type surface band splitting, *Physical Review Letters* **107**,

- 156803 (2011).
- [46] D. Go, J.-P. Hanke, P. M. Buhl, F. Freimuth, G. Bihlmayer, H.-W. Lee, Y. Mokrousov, and S. Blügel, Toward surface orbitronics: giant orbital magnetism from the orbital Rashba effect at the surface of *sp*-metals, *Scientific Reports* **7**, 46742 (2017).
- [47] G. Bihlmayer, S. Blügel, and E. V. Chulkov, Enhanced Rashba spin-orbit splitting in Bi/Ag (111) and Pb/Ag (111) surface alloys from first principles, *Physical Review B* **75**, 195414 (2007).
- [48] F. Meier, H. Dil, J. Lobo-Checa, L. Patthey, and J. Osterwalder, Quantitative vectorial spin analysis in angle-resolved photoemission: Bi/Ag (111) and Pb/Ag (111), *Physical Review B* **77**, 165431 (2008).
- [49] Y. H. Wang, D. Hsieh, D. Pilon, L. Fu, D. R. Gardner, Y. S. Lee, and N. Gedik, Observation of a warped helical spin texture in Bi<sub>2</sub>Se<sub>3</sub> from circular dichroism angle-resolved photoemission spectroscopy, *Physical Review Letters* **107**, 207602 (2011).
- [50] M. Bahramy, P. King, A. De La Torre, J. Chang, M. Shi, L. Patthey, G. Balakrishnan, P. Hofmann, R. Arita, N. Nagaosa, *et al.*, Emergent quantum confinement at topological insulator surfaces, *Nature Communications* **3**, 1159 (2012).
- [51] L. Fu, Hexagonal warping effects in the surface states of the topological insulator Bi<sub>2</sub>Te<sub>3</sub>, *Physical Review Letters* **103**, 266801 (2009).
- [52] S. Basak, H. Lin, L. A. Wray, S. Y. Xu, L. Fu, M. Z. Hasan, and A. Bansil, Spin texture on the warped Dirac-cone surface states in topological insulators, *Physical Review B* **84**, 121401 (2011).
- [53] M. M. Otrokov, T. V. Menshchikova, I. P. Rusinov, M. G. Vergniory, V. M. Kuznetsov, and E. V. Chulkov, Magnetic extension as an efficient method for realizing the quantum anomalous Hall state in topological insulators, *JETP Letters* **105**, 297 (2017).
- [54] H. Tan, D. Kaplan, and B. Yan, Momentum-inversion symmetry breaking on the Fermi surface of magnetic topological insulators, *Physical Review Materials* **6**, 104204 (2022).
- [55] P. M. Sheverdyayeva, C. Hogan, G. Bihlmayer, J. Fujii, I. Vobornik, M. Jugovac, A. K. Kundu, S. Gardonio, Z. R. Benher, G. D. Santo, *et al.*, Giant and tunable out-of-plane spin polarization of topological antimonene, *Nano Letters* **23**, 6277 (2023).
- [56] I. Klimovskikh, S. Eremeev, D. Estyunin, S. Filnov, K. Shimada, V. Golyashov, N. Solovova, O. Tereshchenko, K. Kokh, A. Frolov, *et al.*, Interfacing two-dimensional and magnetic topological insulators: Bi bilayer on MnBi<sub>2</sub>Te<sub>4</sub>-family materials, *Materials Today Advances* **23**, 100511 (2024).
- [57] T. Ozaki, Variationally optimized atomic orbitals for large-scale electronic structures, *Physical Review B* **67**, 155108 (2003).
- [58] T. Ozaki and H. Kino, Numerical atomic basis orbitals from H to Kr, *Physical Review B* **69**, 195113 (2004).
- [59] T. Ozaki and H. Kino, Efficient projector expansion for the *ab initio* LCAO method, *Physical Review B* **72**, 045121 (2005).
- [60] N. Troullier and J. L. Martins, Efficient pseudopotentials for plane-wave calculations, *Physical Review B* **43**, 1993 (1991).
- [61] J. P. Perdew, K. Burke, and M. Ernzerhof, Generalized gradient approximation made simple, *Physical Review Letters* **77**, 3865 (1996).
- [62] S. L. Dudarev, G. A. Botton, S. Y. Savrasov, C. J. Humphreys, and A. P. Sutton, Electron-energy-loss spectra and the structural stability of nickel oxide: An *lsda+u* study, *Physical Review B* **57**, 1505 (1998).
- [63] T. Iwata, T. Kousa, Y. Nishioka, K. Ohwada, K. Sumida, E. Annese, M. Kakoki, K. Kuroda, H. Iwasawa, M. Arita, S. Kumar, A. Kimura, K. Miyamoto, and T. Okuda, Laser-based angle-resolved photoemission spectroscopy with micrometer spatial resolution and detection of three-dimensional spin vector, *Scientific Reports* **14**, 127 (2024).